Jefferson Lab PAC16
Proposal Cover Sheet

This document must be received by close of business Tuesday,

June 08, 1999 at:

Jefferson Lab
User Liaison,
Mail Stop 12B
12000 Jefferson Ave.
Newport News, VA
23606

Experimental Hall: A

Days Requested for Approval: 30

Proposal Title:

Precision Measurement of the Neutron Asymmetry A_1^n at Large x using CEBAF at 6 GeV.

Proposal Physics Goals

Indicate any experiments that have physics goals similar to those in your proposal. Approved, Conditionally Approved, and/or Deferred Experiment(s) or proposals:

Update to E94-101

Contact Person

Name: Zein-Eddine Meziani
Institution: Temple University
Address: Department of Physics, Barton Hall A323
Address: 1900 North 13th Street
City, State, ZIP/Country: Philadelphia, PA 19122
Phone: (215)204-5971 Fax: (215)204-5652
E-Mail: meziani@vm.temple.edu

Jefferson Lab Use Only

Receipt Date: 6/8/99

By: MJX

PR 99-117

BEAM REQUIREMENTS LIST

JLab Proposal No.: E94-101 Date: 06-07-99

Hall: A Anticipated Run Date: 2000-2001 PAC Approved Days: _____

Spokesperson: J.-P. Chen, Z.-E. Meziani and P. Souder Hall Liaison: Jian Ping Chen
Phone: (757)269-7413, (215)204-5971 and (315)443-9102
E-mail: jpchen@jlab.org, meziani@vm.temple.edu,souder@suhep.phy.syr.edu

List all combinations of anticipated targets and beam conditions required to execute the experiment. (This list will form the primary basis for the Radiation Safety Assesment Document (RSAD) calculations that must be performed for each experiment.)

Condition No.	Beam Energy (MeV)	Mean Beam Current (A)	Polarization and Other Special Requirements (e.g., time structure)	Target Material (use multiple rows for complex targets — e.g., w/windows)	Material Thickness (mg/cm^2)	Est. Beam-On Time for Cond. No. (hours)
1	6000	15	Polar. : 80%	^{3}He	50	450
	6000	15		glass windows	44	
2	1600	15	Polar. : 80%	^{3}He	50	50
	1600	15		glass windows	44	

The beam energies, E_{Beam} available are: $E_{Beam} = N \times E_{Linac}$ where N = 1, 2, 3, 4, or 5. E_{Linac} = 800 MeV, i.e., available E_{Beam} are 800, 1600, 2400, 3200, and 4000 MeV. Other energies should be arranged with the Hall Leader before listing.

HAZARD IDENTIFICATION CHECKLIST

JLab Proposal No.: E-94-101 Date : 06/07/99

(For CEBAF User Liaison Office use only.)

Check all items for which there is an anticipated need.

Cryogenics
- _____ beamline magnets
- _____ analysis magnets
- _____ target
  - type: _____
  - flow rate: _____
  - capacity: _____

Electrical Equipment
- _____ cryo/electrical devices
- _____ capacitor banks
- _____ high voltage
- _____ exposed equipment

Radioactive/Hazardous Materials

List any radioactive or hazadorous/ toxic materials planned for use:

_____
_____
_____
_____

Pressure Vessels
- 19cm inside diameter
- 13 atm operating pressure
- Glass window material
- 100 microns window thickness

Flammable Gas or Liquids
- type: _____
- flow rate: _____
- capacity: _____

Drift Chambers
- type: _____
- flow rate: _____
- capacity: _____

Other Target Materials
- ___ Beryllium (Be)
- ___ Lithium (Li)
- ___ Mercury (Hg)
- ___ Lead (Pb)
- ___ Tungsten (W)
- ___ Uranium (U)
- x Other (list below)

  ^3He, N_2, Rb

Vacuum Vessels
- _____ inside diameter
- _____ operating pressure
- _____ window material
- _____ window thickness

Radioactive Sources
- _____ permanent installation
- _____ temporary use
- type: _____
- strength: _____

Large Mech. Structure/System
- _____ lifting devices
- _____ motion controllers
- _____ scaffolding or
- _____ elevated platforms

Lasers
- type: Laser Diode System
- wattage: 7X30 W
- class: IV

Installation:
- x permanent *
- _____ temporary

*for experiment

Use:
- _____ calibration
- _____ alignment

for Polarized ^3He Target

Hazardous Materials
- ____ cyanide plating materials
- ____ scintillation oil (from)
- ____ PCBs
- ____ methane
- ____ TMAE
- ____ TEA
- ____ photographic developers
- ____ other (list below)

_____
_____

General:

Experiment Class:
- x Base Equipment
- _____ Temp. Mod. to Base Equip.
- _____ Permanent Mod. to Base Equipment
- _____ Major New Apparatus

Other: Polarized ^3He target with laser hut

June 1, 1999

Members of the Physics Advisory Committee
TJNAF
12000 Jefferson Avenue
Newport News, VA

Dear PAC-16 Members:

We are sending this update of JLab proposal E94-101, which describes a measurement of the neutron spin-structure asymmetry A_1^n at large x. We wish to have the rating of the experiment upgraded and to request a running time of 30 days as opposed to the 21 days approved.

We feel that this experiment is becoming increasingly highly motivated. A recent review of the topic by Isgur states that if our present understanding of the nucleon in terms of constituent quarks is valid, A_1^n must become significantly positive at kinematics accessible at JLab. On the other hand, all present data is consistent with A_1^n being negative. We feel that it is urgent that this issue be resolved. We now know that data obtained at several other labs has insufficient statistics to provide relevant information. This is an issue where JLab can make a unique and vital contribution.

The PAC13 awarded 21 days of beam, which is sufficient for two points at $x = 0.52$ and 0.63. These data will be sufficient to determine if A_1^n becomes positive, which will represent a major progress in the field. However, the addition of two more points at $x = 0.33$ and 0.42 will use a modest amount of extra time but will provide a measure of the slope of $A_1(x)$ and allow a crude extrapolation to $x \rightarrow 1$. Such information will enhance the impact of the two data points at higher x.

Sincerely,

J.-P. Chen
Z.-E. Meziani
P.Souder
Spokespeople of E94-101

Appendix D (Continued)

Proposal: E-94-101 (Update)

Scientific Rating: B

Spokesperson(s): Z.-E. Meziani, P. A. Souder

Title: Precision Measurement of the Neutron Asymmetry A_1^n at Large x Using JLab at 6 GeV

Motivation:

E-94-101 Update proposes to measure the spin asymmetry A_1^n in inclusive inelastic electron scattering at 6 GeV for a set of points: $0.25 < X_{B_j} < 0.63$ at $2.5 < Q^2 < 5.3$ $(\mathrm{GeV/c})^2$. Models predict this asymmetry to be large and positive as x approaches 1. Existing data do not yet exhibit this behavior for x <0.4. This measurement should clarify the high x behavior of A_1^n.

Measurement and Feasibility:

The experimental technique uses an 80% polarized electron beam at a modest current (15 microamps) at a beam energy of 6 GeV. The target is a polarized ^3He gas cell pressurized to 10 atmospheres in glass and pumped to 40% polarization by 100 watts of diode laser power. These techniques have been (mostly) implemented in previous experiments at other labs. Achieving this high-beam energy and high beam and target polarization are required for E-94-101 to achieve its stated precision. Experimental corrections due to nuclear effects in ^3He, Fermi motion, and radiative effects must be promptly made, but they are not expected to be large at the proposed x values.

Issues:

Since the original conditional approval in 1994, there have been several other experiments on A_1^n at SLAC, CERN, and DESY. The experiments E142, E143, E154, SMC, and HERMES have established good experimental values for A_1^n for values of x <0.4. For the neutron sum rule, the high x region does not contribute significantly to the integral of g_1^n over x. (Both the Ellis-Jaffe Sum Rule and the Bjorken Sum Rule are well measured.) This proposal will not significantly add to or improve this situation. The main objective of E-94-101 Update is to obtain high statistics at large x. The PAC feels the basic physics goals could be met with fewer x points.

Recommendation:

Approval for 21 days.

Proposal: PR-94-101, Hall A

Spokespersons: Z.-E. Meziani & P.A. Souder

Title: Precision Measurement of the Neutron Asymmetry A_1^n at large x_{Bj} using CEBAF at 6 GeV

Motivation:

It is proposed to measure the deep inelastic neutron asymmetry A_1^n at large x using a polarized ^{3}He target and the 6 GeV CEBAF polarized beam. Such a measurement is complementary to the high energy experiments at DESY and SLAC. A_1^n at large x is predicted to be large and positive.

Measurements and Feasibility:

The PAC rates the physics motivation as high and accepts that a measurement of the quality proposed would have a significant impact on our understanding of nucleon structure. As the CEBAF maximum energy rises to and above 6 GeV, the inclusive deep inelastic window opens to allow a number of significant measurements on nucleon structure. The proposal capitalizes on this feature. As proposed, the experiment is judged to be feasible, but the PAC is of the opinion that it is not optimized.

Issues:

The projected results are obtained assuming delivery of high polarization, high intensity electron beam and routine operation of the polarized target for many months. Both of these assumptions have to be demonstrated. In addition, the PAC cautions that the extraction of g_1^n from the precise measurement on ^{3}He may be complicated by the corrections for the D-state admixture in the nuclear ground state. Further, the PAC was not convinced that the spectrometer arrangement was optimized for the proposed measurement. These issues must be resolved before approval could be given to this ambitious, high impact experiment.

Recommendation:

Conditional approval.

Update of TJNAF proposal E94-101

PRECISION MEASUREMENT OF THE NEUTRON ASYMMETRY A_1^n AT LARGE x_{Bj} USING TJNAF AT 6 GeV

B. Filippone, J. Gao, E. Hughes, C. Jones, R. Mckeown, D. Pripstein
California Institute of Technology, Pasadena, CA 91125

D. Margaziotis
California State University, Los Angeles, CA, 90032

J.P. Chen (*Co-spokesperson*), E. Chudakov, J. Gomez, O. Hansen, K. de Jager, M. Kuss
M. Liang, N. Liyanage, J. LeRose, R. Michaels, J. Mitchell, S. Nanda, A. Saha, B. Wojtsekhowski
Thomas Jefferson National Accelerator Facility, Newport News, Virginia 23606

B. Anderson, R. Madey, M. Katramatou, D. M. Manley, G.G. Petratos, D. Prout,
J. W. Watson, W.-M. Zhang
Kent State University, Kent, OH 44242

D. Dale, W. Korsch, P. Zolnierczuk
University of Kentucky, Lexington, KY 40506

D. Dutta, H. Gao
Massachusetts Institute of Technology, Cambridge, MA 02139

J. Calarco
University of New Hampshire, Durham, NH 03824

G.D. Cates, K. Kumar
Princeton University, Princeton, NJ 08544

E. Brash
University of Regina, Regina, SK, S4S OA2

C. Glashausser, R. Gilman, X. Jiang, G. Kumbartzki, R.D. Ransome, S. Strauch
Rutgers University, Rutgers, NJ 08855

R. Holmes, J. McCracken, P.A. Souder(*Co-spokesperson*)
Syracuse University, Syracuse, NY 13122

L. Auerbach, S. Choi, Z.-E. Meziani(*Spokesperson*)
Temple University, Philadelphia, PA 19122
M. Finn, T. Averett
The College of William and Mary, Williamsburg, VA 23185

P. Bertin, Y. Roblin
University Blaise Pascal, Clermont-Ferrand, France

and

The Hall A collaboration

Abstract

We propose to carry out a determination of the deep inelastic neutron asymmetry A_1^n in the large x region ($0.33 \leq x \leq 0.63$) and at reasonably high Q^2 ($3.2 \leq Q^2 \leq 5.3$), from a measurement using a high pressure polarized ^{3}He target and the polarized beam at the highest available JLab energy 6 GeV. The precision attainable at JLab is unchallenged by any of the world high energy facilities (SLAC, CERN, HERMES) engaged in the measurement of this quantity. All measurements carried out to-date display a poor statistical uncertainty for $x \geq 0.4$. At JLab we are in a unique position to obtain a measurement of A_1^n with much higher precision for $x \geq 0.5$ than previously possible. All present data is consistent with $A_1^n < 0$,. However, as first pointed out by Feynman and Close, very general arguments based on the quark structure of the nucleon predict that as $x \rightarrow 1$, $A_1^n(x) \rightarrow +1$. Moreover, for $x > 0.5$, A_1^n should be positive. Our experiment has the sensitivity to determine if this dramatic prediction is valid.

We request a total of 30 days to carry out this measurement.

1 Physics Motivation

1.1 Introduction

We are proposing to measure the asymmetry A_1^n in the deep inelastic scattering of polarized electrons from the polarized neutron in ^{3}He at large Bjorken x. If one examine the presently available neutron world data [1, 2, 3, 4, 5, 12] of this quantity one notice their poor statistical accuracy in the large x region ($x \geq 0.5$). At JLab, we are in a unique position to obtain a measurement of A_1^n with much higher precision for $x \geq 0.5$. Furthermore, all present data is consistent with $A_1^n < 0$. However, as first pointed out by Feynman [6] and Close [7], very general arguments based on the quark structure of the nucleon predict that as $x \to 1$, $A_1^n(x) \to +1$. Moreover, A_1^n is predicted to be positive for $x > 0.5$. Our experiment has the sensitivity to determine if this important prediction is valid.

In our original proposal we requested 43 days to carry a measurement with data points at 6 different x values. Only 21 days were approved and the experiment was rated B. Since then, most of the world experiments have been completed and the statistical precision in the large x region has not improved to resolve the physics issue addressed in this proposal. SLAC experiment E154 still provides the neutron result with the smallest statistical uncertainty in the large x region. SLAC experiment E155, while designed for a higher precision measurement on the proton and deuteron, is not expected to do better than SLAC-E154 for the neutron result. It still suffers from the same limitations in order to perform a good measurement in the large x region, as the other high energy facilities experiments. Finally, we should also point out that experiment E93-009 of Hall B is aiming at measuring the extended GDH sum, the same goals as experiment E94-010 of Hall A. It does not measure the deep inelastic high x region.

Furthermore, the recent successful completion of two polarized beam, polarized ^{3}He target experiments in Hall A at JLab, demonstrates the feasibility of the experiment proposed here. We believe that the present experimental situation as well as the new theoretical developments, which will be discussed later, warrant a re-evaluation of this proposal. From our side we have optimized the choice of kinematics to be $0.33 \leq x \leq 0.63$ with four points and a modest increase of 9 days in beam time for a maximum physics impact.

1.2 Deep Inelastic Scattering in the Quark-Parton Model

The cross section for spin-independent deep inelastic scattering (DIS) is given by

$$\frac{d\sigma}{dxdy} = \frac{2\pi x^2}{Q^4} s[1 + (1-y)^2] F_2(x) \tag{1}$$

where

$$F_2(x) = \sum x e_i^2 f_i(x). \tag{2}$$

Here we have used the usual variables $\nu = E - E'$, $x = Q^2/2M_n\nu$, $y = \nu/E$, and $s = M_n E$.

The quantity x is interpreted as the fraction of momentum carried by struck quark. The physics is in the quark momentum distributions $f_i(x)$, which give the probability that the i^{th} quark of charge e_i carries a fraction x of the momentum of the nucleon in the infinite momentum frame. For this discussion, we neglect the contribution of longitudinal photons to the cross section. The details of how to include these effects is presented later. The cross section corresponds to a virtual photon being absorbed by a single quark as shown in Fig.1.

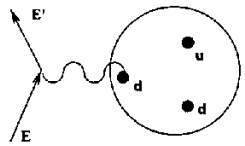

Figure 1: Diagram for Deep Inelastic Scattering from the neutron.

For spin-dependent scattering, the momentum distributions can be decomposed into spin states:

$$f_i(x) = \frac{1}{2}\Big(q_i^{\uparrow}(x) + q_i^{\downarrow}(x)\Big); \quad g_i(x) = \frac{1}{2}\Big(q_i^{\uparrow}(x) - q_i^{\downarrow}(x)\Big) \tag{3}$$

where the $\uparrow$ ($\downarrow$) refers to the quark spin being parallel(antiparallel) to the spin of the nucleon. The asymmetry that we plan to measure is most simply defined in terms of scattering at $\theta = \pi$, where we have

$$A_1(x) = \frac{d\sigma^{\uparrow\downarrow} - d\sigma^{\uparrow\uparrow}}{d\sigma^{\uparrow\downarrow} + d\sigma^{\uparrow\uparrow}}\bigg|_{180^\circ} = \frac{g_1(x)}{f_1(x)} \tag{4}$$

here $d\sigma^{\uparrow\downarrow}$ ($d\sigma^{\uparrow\uparrow}$) is the scattering cross section of polarized electron beam off polarized target with helicities of the beam and target antiparallel (parallel). For less backward angles, the major effect on the asymmetry is a kinematic depolarization factor $D < 1$ defined later.

1.3 SU(6) and Broken SU(6) Predictions

To first approximation, the constituent quarks in the nucleon are described by the SU(6) wave-functions shown in Fig. 2. The only assumptions are that isospin and spin are 1/2 and that the non-color part of the wavefunction is perfectly symmetric. More explicitely the wave function of a neutron polarized in the $+z$ direction has the form [7]:

$$\begin{aligned} |n\uparrow\rangle \;=\; & \frac{1}{\sqrt{2}}\,|d\uparrow(ud)_{S=0}\rangle \;+\; \frac{1}{\sqrt{18}}\,|d\uparrow(ud)_{S=1}\rangle \;-\; \frac{1}{3}\,|d\downarrow(ud)_{S=1}\rangle \\ & -\frac{1}{3}\,|u\uparrow(dd)_{S=1}\rangle \;-\; \frac{\sqrt{2}}{3}\,|u\downarrow(dd)_{S=1}\rangle\,, \end{aligned} \tag{5}$$

where the subscript S denotes the total spin of the two-quark component. For the case of the proton one needs to merely exchange the u and d quarks. In this limit where SU(6) is an exact symmetry, both "diquark"-spin states $S = 1$ and $S = 0$ contribute equally to the observables of interest, leading to the three predictions:

$$R^{np} \equiv \frac{F_2^n}{F_2^p} = \frac{2}{3}; \quad A_1^p = 5/9; \quad \text{and} \quad A_1^n = 0. \tag{6}$$

Data for these quantities are shown in Fig. 3. A qualitative success of SU(6) is displayed in the region $x > 0.4$, for $A_1^p(x)$, where the data are consistent with 5/9. Also $A_1^n(x)$ is consistent with being small (but negative) everywhere.

On the other hand, data for R^{np} agree poorly with the SU(6) prediction. $R^{np}(x)$ is a straight line but with a big slope starting with $R^{np}(0) = 1$ but dropping to approximately $R^{np}(1) = 1/4$. In addition, $A_1^p(x)$ is small at low x. The fact that $R(0) = 1$ and $A_1^p(0) \sim 0$ may be explained by the presence of copious sea quarks that are similar for protons and neutrons and are not highly polarized. At high x, however, there are few sea quarks and there must be some problem with the SU(6) wavefunction.

A natural explanation based on phenomenological arguments [7, 13] is an SU(6)-breaking suppression of the "diquark" configurations in equation (5) having $S = 1$ relative to the $S = 0$ configuration. Such a splitting has an obvious dynamical origin, namely the large hyperfine interaction among the quarks:

$$\vec{S}_i \cdot \vec{S}_j \delta^3(\vec{r}_{ij}). \tag{7}$$

It is this interaction that explains, for example, the $N - \Delta$ splitting. The effect of the perturbation on the wavefunction is to lower the energy of the $S = 0$ "diquarks", allowing the d-quark in the first term of equation (5), which has its spin parallel to that of the neutron, to be more energetic and hence to dominate the high energy tail of the quark momentum distribution that is probed

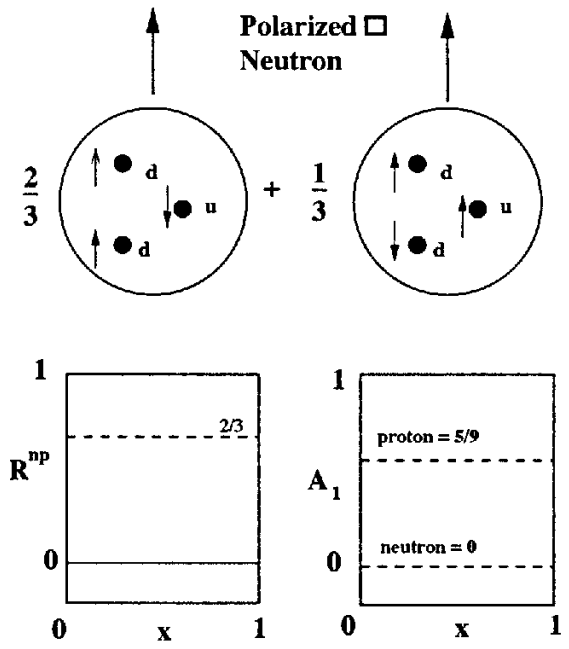

Figure 2: Top: Probabilities for spin configurations of the SU(6) wavefunction for the neutron. Bottom left: Prediction for R^{np} in SU(6). Bottom right: Prediction for $A_1(x)$ in SU(6) for both proton and neutron.

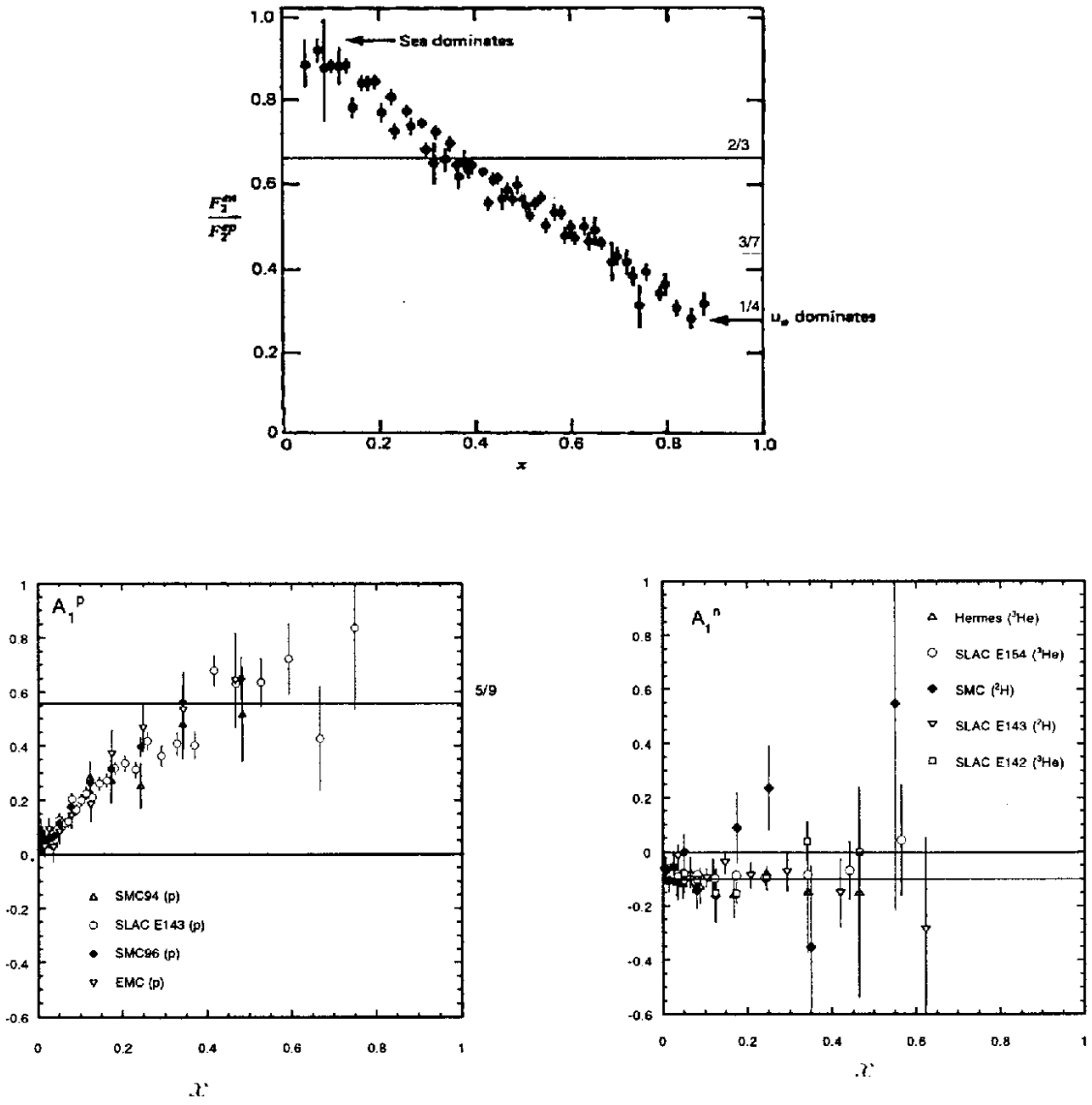

Figure 3: Top: F_2^n/F_2^p as a function of x ratio extracted from the SLAC measurements of proton and deuteron in deep inelastic scattering. Bottom left: World proton data A_1^p versus x from Ref.[8, 9, 2, 10, 3, 11]. Bottom right: World neutron data A_1^n versus x from Ref.[1, 2, 3, 4, 5]. Notice the linear scale in x.

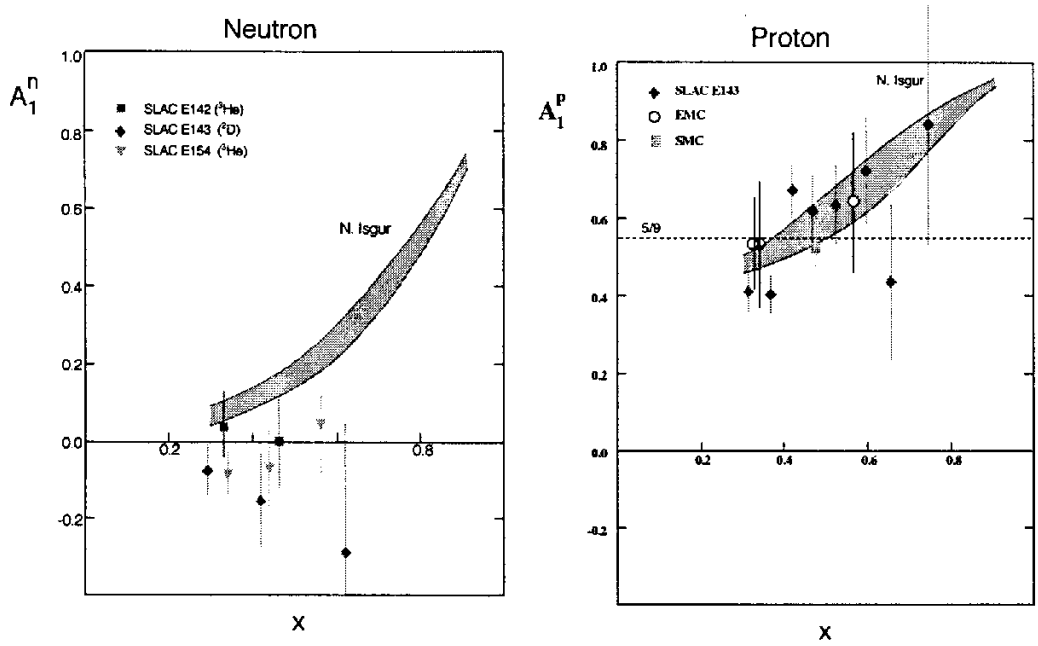

Figure 4: Left: Prediction of A_1^n versus x as evaluated in Ref. [14]. Right: Same as left but for the proton. Note that the predictions of SU(6) are $A_1^n = 0$ and $A_1^p = 5/9$.

near $x = 1$. The dominance of this term as $x \to 1$ implies:

$$R^{np} \to \frac{1}{4}; \quad A_1^p \to 1; \quad \textit{and} \quad A_1^n \to 1. \tag{8}$$

If indeed this specific SU(6) symmetry breaking is the explanation for the behavior of $R^{np}(x)$, then there are also predictions for $A_1^p(x)$ and $A_1^n(x)$ as shown in Fig. 4. As recently pointed out by Isgur [14], there is little freedom in the predictions if quarks with broken SU(6) symmetry are a useful description of the nucleon. Unfortunately, the data on $A_1^{n,p}$ at high x lacks the precision even to distinguish this prediction from the simple SU(6) prediction.

One question is how we use a heavy, nonrelativistic, constituent quark picture to predict the properties of quarks seen in DIS, which probes the light current quarks at high Q^2. A natural answer is, that we will probe the light quark inside the constituent quark. For constituent quarks, $A_1^q = 1$ at high x.

1.4 PQCD

Another approach focuses directly on relativistic quarks instead of the nonrelativistic quarks of the above discussion. Farrar and Jackson[15, 16] in the early 70's, as one of the first applications of PQCD, noted that at $x \to 1$, the scattering is from a high energy quark, and the process can be treated perturbatively. Farrar and Jackson proceeded to show that a quark carrying nearly all the momentum of the nucleon (i.e. $x \to 1$) must have the same helicity as the nucleon and that quark-gluon interactions cause only the $S = 1$, $S_z = 1$ diquark spin projection component, rather than the full $S = 1$ diquark system to be suppressed as $x \to 1$.

$$d^{\downarrow} = u^{\downarrow} = 0; \quad \frac{d^{\uparrow}}{u^{\uparrow}} \rightarrow \frac{1}{5} \quad \Rightarrow A_1(1) \rightarrow 1 \tag{9}$$

They obtained the previous limiting value for both the proton and the neutron, namely $A_1^{n,p} \rightarrow 1$ for $x \rightarrow 1$. Note that in this theory $R^{np} \rightarrow 3/7$ versus $1/4$ for the constituent quarks. A similar result is obtained in the treatment of Brodsky and collaborators [17] based on quark-counting-rules.

This is one of few places where QCD can provide for an absolute prediction about structure functions (here a ratio of structure functions). How low in x this picture works is uncertain.

1.5 A_1^n and the Spin Crisis

As pointed out by Isgur [14] a precision measurement of both A_1^n and A_1^p is relevant in confirming that the valence quark spin distributions are "normal".

The current situation of the spin crisis, based on violations of the Ellis-Jaffe sum rule, is that the net spin

$$\Sigma = \Sigma_v + \sum_q \Delta(q + \overline{q})_{sea} \sim 0.3 \pm 0.1 \tag{10}$$

carried by all quarks and antiquarks, valence and sea, is significantly less than the naive prediction of 1. The basic valance quark models predict $\sigma_v \sim 0.75$, where the drop from 1 is due to relativistic effects. Also, the spin-structure function data suggest that $\Delta(q+\overline{q})_{sea} = -0.45$ could be reasonable. This gives a consistent picture. One obvious constraint is:

$$\Sigma_v + \sum_q \Delta(q + \overline{q})_{sea} + 2L_q + \Sigma_g = 1 \tag{11}$$

where L_q is the quark orbital angular momentum and Σ_g is the total contribution form gluons. Measuring Δg and $\Delta\overline{q}$ is high priority for various experiments planned or underway at HERMES, RHIC and CERN. The plan is to gain as complete a picture of what carries angular momentum in the nucleon as possible. However, the implicit foundation of this program is knowing the contribution of the valence quarks. Measuring A_1^n checks our understanding of Σ_v. If $A_1(x)$ maintains its present trend and remains negative at high x, this will cast grave doubt on our theory of the large contribution from valence quarks.

Finally, we note that recently Kochelev [18] has proposed an approach to interpreting the nucleon with QCD that includes instantons as an important degree of freedom. With this radically different picture, the prediction is that $A_1^n(x)$ remains negative or close to zero [19].

In summary, while data on $R^{n,p}$ and A_1^p indicate to some extent the predicted x dependence for these quantities in the large x region, the experimental situation for the neutron A_1^n is much less clear. The statistical precision of the data at present, does not allow a meaningful statement about the behavior of A_1^n in the large x region. Our motivation is to perform a precision measurement of the neutron structure function in the large x region which will undoubtedly give us insight into the dynamics of partons in the nucleon.

1.6 Cross sections and Asymmetries

In deep-inelastic electron scattering, the measured longitudinal asymmetry $A^{\parallel}$ is determined experimentally from measurements of cross sections for polarized electrons on polarized nucleons between states where the helicity are parallel and antiparallel[20, 21]:

$$A^{\parallel} = \frac{\sigma^{\uparrow\downarrow} - \sigma^{\uparrow\uparrow}}{\sigma^{\uparrow\downarrow} + \sigma^{\uparrow\uparrow}} = \frac{1-\epsilon}{(1-\epsilon R)\ W_1(Q^2,\nu)}\ [M(E+E'\cos\theta)\ G_1(Q^2,\nu) - Q^2 G_2(Q^2,\nu)] \quad (12)$$

Here $\sigma^{\uparrow\uparrow}$ ($\sigma^{\downarrow\uparrow}$) is the inclusive $d^2\sigma^{\uparrow\uparrow}/d\Omega d\nu$ ($d^2\sigma^{\downarrow\uparrow}/d\Omega d\nu$) differential scattering cross section for longitudinal target spins parallel (antiparallel) to the incident electron spins. A corresponding relationship exists for scattering of longitudinally polarized electrons off a transversely polarized target where the transverse asymmetry is defined by[21]:

$$A^{\perp} = \frac{\sigma^{\downarrow\leftarrow} - \sigma^{\uparrow\leftarrow}}{\sigma^{\downarrow\leftarrow} + \sigma^{\uparrow\leftarrow}} = \frac{(1-\epsilon)E'}{(1-\epsilon R)\ W_1(Q^2,\nu)}[(MG_1(Q^2,\nu) + 2EG_2(Q^2,\nu))\ \cos\theta] \quad (13)$$

where R is the ratio of longitudinal-to-transverse virtual-photo-absorption cross sections

$$R = \frac{W_2}{W_1}\ \left(1 + \frac{\nu^2}{Q^2}\right) - 1 \quad (14)$$

and ϵ is the virtual photon polarization;

$$\epsilon = \left[1 + 2\left(1 + \frac{\nu^2}{Q^2}\right)\tan^2\frac{\theta}{2}\right]^{-1} \quad (15)$$

Here $\sigma^{\downarrow\leftarrow}(\sigma^{\uparrow\leftarrow})$ is the inclusive scattering cross section for beam-spin antiparallel (parallel) to the beam momentum, and for target-spin direction transverse to the beam momentum and towards the direction of the scattered electron. In all cases, G_1 and G_2 are the spin-dependent structure functions, whereas W_1 and W_2 are the spin-averaged structure functions; M is the mass of the nucleon; Q^2 is the square of the four-momentum of the virtual photon; E is the incident electron energy; E' is the scattered electron energy; $\nu = (E - E')$ is the electron energy loss; and θ is the electron scattering angle.

The experimental asymmetries $A^{\parallel}$ and $A^{\perp}$ are related to the virtual photon-nucleon longitudinal and transverse asymmetries A_1 and A_2 by the relations

$$A^{\parallel} = D(A_1 + \eta A_2) \quad (16)$$
$$A^{\perp} = d(A_2 - \zeta A_1) \quad (17)$$

where D, d, η and ζ are defined as follows

$$D = (1 - E'\epsilon/E)/(1+\epsilon R) \quad (18)$$
$$d = D\sqrt{2\epsilon/(1+\epsilon)} \quad (19)$$
$$\eta = \epsilon\sqrt{Q^2}/(E - E'\epsilon) \quad (20)$$
$$\zeta = \eta(1+\epsilon)/2\epsilon \quad (21)$$

The depolarization factor D gives the target polarization projection along the direction of the virtual photon vector $\vec{q}$.

In the scaling limit (ν and Q^2 large), the structure functions in Eqs. (12) and (13) are predicted to depend only on the Bjorken variable $x = Q^2/2M\nu$, yielding

$$MW_1(\nu, Q^2) \rightarrow F_1(x) \quad (22)$$
$$\nu W_2(\nu, Q^2) \rightarrow F_2(x) \quad (23)$$
$$M^2\nu G_1(\nu, Q^2) \rightarrow g_1(x) \quad (24)$$
$$M\nu^2 G_2(\nu, Q^2) \rightarrow g_2(x) \quad (25)$$
$$(26)$$

The quantities to be determined in this experiment are A_1 and A_2. They can be expressed in terms of the measured quantities as:

$$A_1 = \frac{\sigma^T_{1/2} - \sigma^T_{3/2}}{\sigma^T_{1/2} + \sigma^T_{3/2}} = \frac{\sigma_{TT}}{\sigma_T} = \frac{A_\parallel}{D(1+\eta\zeta)} - \frac{\eta A_\perp}{d(1+\eta\zeta)} = \frac{g_1(x,Q^2) - \gamma^2 g_2(x,Q^2)}{F_1(x,Q^2)}$$
$$A_2 = \frac{2\sigma_{LT}}{\sigma^T_{1/2} + \sigma^T_{3/2}} = \frac{\sigma_{LT}}{\sigma_T} = \frac{\zeta A_\parallel}{D(1+\eta\zeta)} + \frac{A_\perp}{d(1+\eta\zeta)} = \frac{\gamma(g_1(x,Q^2) + g_2(x,Q^2))}{F_1(x,Q^2)}, \quad (27)$$

where $\sigma^T_{1/2}$ and $\sigma^T_{3/2}$ are the virtual photoabsorption transverse cross sections for total helicity between photon and nucleon of 1/2 and 3/2 respectively, σ_{LT} is the interference term between the transverse and longitudinal photon-nucleon amplitudes, $\sigma_T = (\sigma^T_{1/2} + \sigma^T_{3/2})/2$, and $\sigma_{TT} = (\sigma^T_{1/2} - \sigma^T_{3/2})/2$.

Within the QPM interpretation, $F_1^n(x)$ and $g_1^n(x)$ are related to the momentum distribution of the constituents as

$$F_1(x) = \frac{1}{2}\sum_{i=1}^{f} e_i^2 \left[q_i^\uparrow(x) + q_i^\downarrow(x)\right] \quad (28)$$
$$g_1(x) = \frac{1}{2}\sum_{i=1}^{f} e_i^2 \left[q_i^\uparrow(x) - q_i^\downarrow(x)\right] \quad (29)$$

where i runs over the number of flavors, e_i are the quark fractional charges, and $q_i^\uparrow$, $(q^\downarrow)_i$ are the quark plus antiquark momentum distributions for quark and antiquarks spins parallel (antiparallel) to the nucleon spin.

$g_2^n(x)$ has no simple interpretation in the QPM but contain information on the quark-gluon correlations.

1.7 Why at JLab?

From an experimental viewpoint the measurement of the nucleon spin structure function at large x presents challenges when attempted at the high energy machines (CERN, HERA and SLAC). A close examination of all the results from these experiments shows clearly the statistical limitation of the measurements in the high x region. In fact for the region $x \geq 0.4$ the statistical uncertainty on the neutron measurement is quite large, starting in the best case around $\Delta A_1^n = \pm 10\%$ at $x = 0.4$ and reaching $\Delta A_1^n = \pm 50\%$ at $x = 0.65$. The large scattered lepton energies (greater than 20 GeV) needed to reach high x (0.4-0.7) combined with the spectrometer resolution and the small cross sections give poor results.

A close look at the kinematical parameters suggests that measurements of asymmetry at large x are best performed at TJNAF with incident energies of 6 GeV and greater.

- The high duty cycle and high current of TJNAF compensate for the relatively low density ^{3}He polarized target.

- For large x, the small incident energy of the machine requires a detection of the scattered electron at large angle to reach high x. This in turn provides a large Q^2 but small scattered electron energies due to the large recoil factor. For TJNAF these scattered energies are typically between 1 and 2 GeV leading to a better x resolution compared to any of the high energy spectrometers used around the world.

- The depolarization factor D which is typically about 0.3 at any high energy machine can get as large as 0.85 at TJNAF because of the large scattering angle. This is most advantageous when extracting the physics asymmetry A_1^n from the measured asymmetry $A^{\|}$.

- The lower incident electron energy at TJNAF (compared to the 20-200 GeV elsewhere) increases the Mott cross section, thereby partially compensating for the decrease in cross section at large angles for fixed x.

2 The Experimental procedure

We propose to measure the asymmetry $A_1^{^3He}$ and determine the neutron asymmetry A_1^n with high precision at large x. We shall use the longitudinally polarized ($P_b = 0.8$) high energy TJNAF electron beam ($E_i = 6$ GeV) and a 20-cm-long high pressure double cell polarized ^{3}He target. The target is long enough to keep the glass front and end windows out of the spectrometers target acceptance. The measurement will be performed at one incident electron beam energy ($E_i = 6$ GeV) and both HRS spectrometers in a symmetric configuration at one scattering angle ($\theta = 45°$). Four momentum settings for each spectrometer will cover the range $0.3 \leq x \leq 0.63$ and $Q^2 \geq 2.4$ GeV^2 with $W \geq 2$ GeV. The target polarization orientation can be set longitudinal or transverse to the beam with a value of $P_t = 0.40$. A beam current of 15 μA combined with a target density of 3.5×10^{21}atoms/cm^2 (the target effective length seen by each spectrometer is 14.1cm) offers a

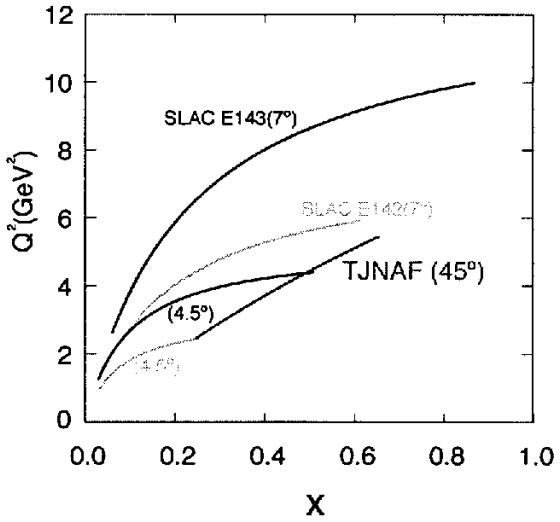

Figure 5: Q^2 versus x kinematics range accessible in this experiment (solid line) compared the the SLAC E-142 and E143 kinematics[1, 3] (dashed line). Notice that in this experiment Q^2 larger than 2 $(GeV)^2$ for all x values.

luminosity of $3.3\text{x}10^{35}$ $\text{cm}^{-2}\text{s}^{-1}$ for the proposed measurement. This allows the measurement to be performed in a time period of 720 hours with beam on target.

2.1 The Polarized Beam

In this proposal we shall assume, that the achievable beam polarization at TJNAF is (80%) with a current of $15\mu A$. While about 70% electron beam polarization has been delivered on a regular basis to E94-010 and E95-001, we are optimistic that by the time this experiment runs and with the experience gained using the strained GaAs cathodes, 80% beam polarization will be achieved. The polarization of the beam will be measured with the Hall A Moller and Compton polarimeters.

2.2 The Polarized ^{3}He Target

The polarized target will be based on the principle of spin exchange between optically pumped alkali-metal vapor and noble-gas nuclei[22, 23, 24]. It is similar to that used in JLab experiment E94-010 and E95-001 in Hall A.

A central feature of the target will be sealed glass target cells, which under operating conditions, will contain a ^{3}He pressure of about 10 atmospheres. As indicated in Fig. 6, the cells will have two chambers, an upper chamber in which the spin exchange takes place, and a lower chamber, through which the electron beam will pass. In order to maintain the appropriate number density of the alkali-metal Rubidium the upper chamber will be kept at a temperature of 170–200 ° using an oven constructed of high temperature plastic Torlon. With a density of 2.5×10^{20} atoms/cm^3, and a lower cell length of 20 cm. With this length the end glass windows are not seen by the spectrometer acceptance when it is set at a scattering angle of 45°. The effective target thickness will be 3.5×10^{21}atoms/cm^2, since the spectrometer acceptance sees a length of 10 cm/$\sin\theta_e$= 14.1cm

The main components of the target are shown in Fig. 6. The main "coils" shown are large Helmholtz coils used to apply a static magnetic field of about 25 Gauss. Also shown are the components for the NMR and EPR polarimetry. The NMR components of the target include a set of RF drive coils, and a separate set of pickup coils. Not shown in the figure are the NMR electronics, which include an RF amplifier, a lock-in amplifier, some bridge circuitry, and the capability to sweep the static magnetic field. The EPR components include an EPR excitation coil and a photodiode for detection of the EPR line. The oven shown in Fig. 6 is constructed of Torlon, a high temperature plastic and is heated with forced hot air. The optics system include a system of 4 diode lasers for longitudinal pumping and 3 for transverse pumping. A polarizing beam splitter, lens system and a quarter wave plate are required to condition each laser beam line and provide circular polarization.

2.2.1 Operating Principles

The time evolution of the ^{3}He polarization can be calculated from a simple analysis of spin-exchange and ^{3}He nuclear relaxation rates[25]. Assuming the ^{3}He polarization $\text{P}_{^3\text{He}} = 0$ at $t = 0$,

$$\text{P}_{^3\text{He}}(\text{t}) = \text{P}_{\text{Rb}} \left(\frac{\gamma_{\text{SE}}}{\gamma_{\text{SE}} + \Gamma_{\text{R}}}\right) \left(1 - \text{e}^{-(\gamma_{\text{SE}}+\Gamma_{\text{R}})\,\text{t}}\right) \tag{30}$$

where γ_{SE} is the spin-exchange rate per ^{3}He atom between the Rb and ^{3}He, Γ_{R} is the relaxation rate of the ^{3}He nuclear polarization through all channels other than spin exchange with Rb, and

P_{Rb} is the average polarization of the Rb atoms. Likewise, if the optical pumping is turned off at $t = 0$ with $P_{^3He} = P_0$, the ^{3}He nuclear polarization will decay according to

$$P_{^3He}(t) = P_0\, e^{-(\gamma_{SE}+\Gamma_R)\,t}. \tag{31}$$

The spin exchange rate γ_{SE} is defined by

$$\gamma_{SE} \equiv \langle \sigma_{SE}\, v \rangle\, [Rb]_A \tag{32}$$

where, $\langle \sigma_{SE}\, v \rangle = 1.2 \times 10^{-19}$ cm^3/sec is the velocity-averaged spin-exchange cross section for Rb–^{3}He collisions[25, 26, 27] and $[Rb]_A$ is the average Rb number density seen by a ^{3}He atom. The target operates with $1/\gamma_{SE} = 8$ hours. From equation (30) it is clear that the best possible ^{3}He polarization is obtained by maximizing γ_{SE} and minimizing Γ_R. But from equation (32) we can see that maximizing γ_{SE} means increasing the alkali-metal number density, which in turn means more laser power. The number of photons needed per second must compensate for the spin relaxation of Rb spins. In order to achieve $1/\gamma_{SE} = 8$ hours, about 50 Watts of usable laser light at a wavelength of 795 nm will be required.

The rate at which polarization is lost is characterized by Γ and has four principle contributions. An average electron beam current of about 15 μA will result in a depolarization rate of $\Gamma_{beam} = 1/30$ hours[28]. The cells produced in previous experiments have typically an intrinsic rate of $\Gamma_{cell} = 1/50$ hours. This has two contributions, relaxation that occurs during collisions of ^{3}He atoms due to dipole-dipole interactions, and relaxation that is largely due to the interaction of the

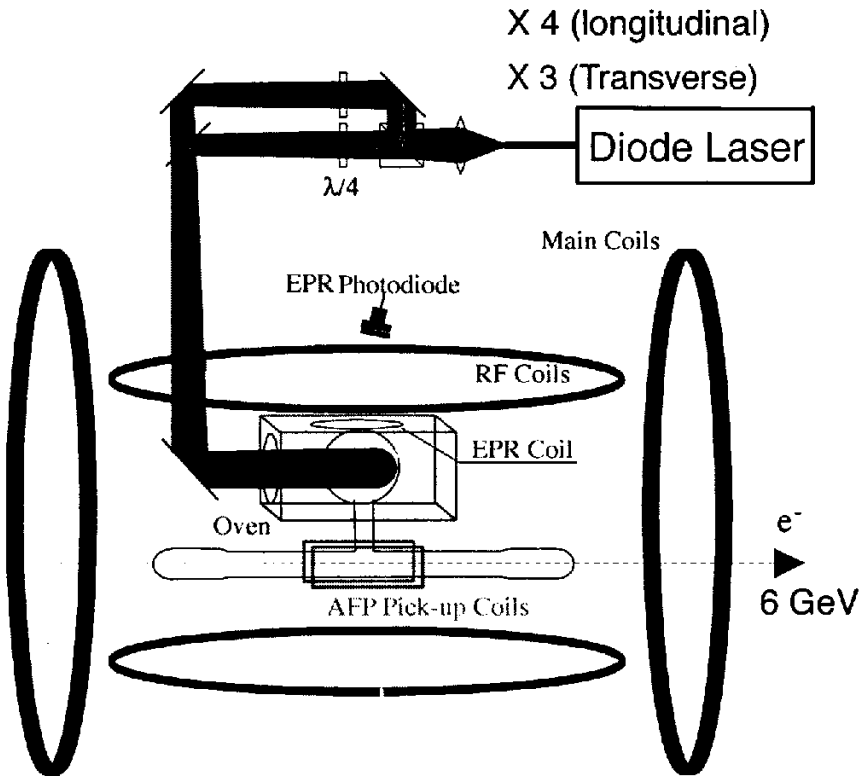

Figure 6: JLab Hall A polarized ^{3}He target setup.

^{3}He atoms with the walls. Finally, relaxation due to magnetic field inhomogeneities was held to about $\Gamma_{\nabla B} = 1/100$ hours. Collectively, under operating conditions, we would thus expect

$$\Gamma_R = \Gamma_{beam} + \Gamma_{cell} + \Gamma_{\nabla B} = 1/30\,\text{hours} + 1/50\,\text{hours} + 1/100\,\text{hours} = 1/16\,\text{hours}.$$

Thus, according to eqn. (30), the target polarization cannot be expected to exceed

$$P_{max} = \frac{\gamma_{SE}}{\gamma_{SE} + \Gamma_R} = 0.66$$

Realistically, a Rb polarization of 100% in the pumping chamber will not be achieved, which will reduce the polarization to about 40%.

During E94-010 and E95-001 we achieved a polarization of about 30-35% when a beam current of 15μA was used. The beam depolarization was slightly larger than expected and this was the first time that such a large beam current was used for an extended period time. We point out that the target was exceptionally long (40 cm). In this experiment the target length is half of that used in E94-010 and E95-001. We expect a significant improvement in polarization due to the favorable ratio of volumes between the pumping and target cells. An R&D effort is underway by JLab and the polarized ^{3}He target collaboration to improve the achievable polarization under the beam conditions proposed in this experiment.

2.2.2 Target Cells

The length of the cell has been chosen to be 20 cm so that the end windows are not within the acceptance of the Hall A spectrometers at 45°. The end windows themselves will be about 100 μ thick. Thinner windows could in principle be used, but this does not appear to be necessary.

2.2.3 The Optics System

As mentioned above, approximately 50 Watt of "usable" light at 795 nm will be required. By "usable", we mean circularly polarized light that can be readily absorbed by the Rb. It should be noted that the absorption line of the Rb has a full width of several hundred GHz at the high pressures of ^{3}He at which we will operate. Furthermore, since we will operate with very high Rb number densities that are optically quite thick, even light that is not well within their absorption line width can still be absorbed.

The laser system is similar to that used in E94-010. It consists of commercially available 30 Watt fiber-coupled diode laser systems. Four such lasers are used to pump along the longitudinal direction and and three along the transverse direction. The efficiency of these lasers has been tested during experiment E94-010 and E95-001 and found to be totally adequate for this experiment needs.

2.2.4 Polarimetry

Polarimetry is accomplished by two means. During the experiment, polarization is monitored using the NMR technique of adiabatic fast passage (AFP)[29]. The signals are calibrated by comparing the ^{3}He NMR signals with those of water. The calibration is then independently verified by studying the frequency shifts that the polarized ^{3}He nuclei cause on the electron paramagnetic resonance (EPR) lines of Rb atoms[28]. Both methods were used in E94-010, very preliminary analysis shows that the NMR measurements with water calibration are consistent with the EPR results.

2.3 The Spectrometers Setup

We plan to use both HRS spectrometers in Hall A. We will the electron spectrometer with its standard detector package for electrons and the hadron spectrometer with an added lead glass calorimeter which was first used in E94-010. Each spectrometer will then consist of;

- Two vertical Drift Chambers (VDCs) for the measurement of momentum and production angle.
- Gas Čerenkov counter for pion rejection.
- A set of scintillators for triggering on charged particles.
- A lead glass calorimeter for additional pion rejection.

As the E94-010 analysis shows, the pion rejection factor with the Čerenkov counter and the lead glass calorimeter are better than $2\text{x}10^{-4}$ which is sufficient for our worst case.

Advantages of this measurement compared to other high energy proposals are;

- The "good electrons" events in the spectrometer are in principle due only to scattering off ^{3}He nuclei. The target cell glass windows are outside the acceptance of the spectrometer
- The excellent target reconstruction by the HRS spectrometers allows for better background rejection.
- The excellent resolution of the spectrometer permits the measurement of elastic scattering off ^{3}He.

2.4 Proposed Measurements and Data Analysis

The measurement consists of collecting data at one incident energy ($\text{E}_i = 6$ GeV) and one scattering angle ($\theta = 45°$) but for six spectrometer momentum settings to cover the range $0.33 \leq x \leq 0.63$.

The raw measured ^{3}He counting asymmetry Δ is converted to the experimental asymmetry $A_{\parallel}^{^3He}$, using the relation

$$A_{\parallel}^{^3He} = \frac{\Delta}{P_b P_t} \tag{33}$$

$$\Delta = \frac{(N^{\uparrow\downarrow} - N^{\uparrow\uparrow})}{(N^{\uparrow\downarrow} + N^{\uparrow\uparrow})} \tag{34}$$

where $N^{\uparrow\downarrow}$ ($N^{\uparrow\uparrow}$) represents the rate of scattered electrons for each bin of x and Q^2 when the electron beam helicity is antiparallel (parallel) to the target spin. $P_b = 0.80$ and $P_t = 0.35$ are the beam and target polarization respectively. The target is long enough (20 cm) so that no dilution of the asymmetry due to its glass windows occurs, however, early in the measurement empty target measurements will be made to insure that no extra dilution of $A_{\parallel}^{^3He}$ occurs from possible background originating in the target area. This study will benefit greatly from the excellent target reconstruction capability of the HRS. The kinematics and electron rates are presented in table 1, where we used a fit of the E-142 data[1] as a model for an estimate of $A_1^{^3He}$, assuming no Q^2 dependence of this asymmetry. We used the unpolarized structure functions from the Whitlow 1990 fits[37] to the deep inelastic measurements on proton and deuteron. We added incoherently the appropriate structure functions to generate the ^{3}He cross sections. The rates where determined assuming for

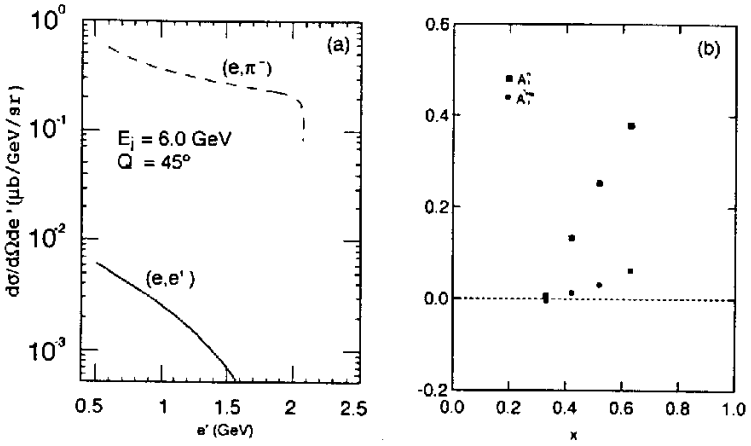

Figure 7: (a)Projected pion and electron cross sections. (b) Projected data for this experiment. Solid circles correspond to the measurement on ^{3}He. The solid squares are the projected extracted neutron asymmetry after proton correction. The neutron asymmetry includes statistical and systematic uncertainties added quadratically.

each of the electron and hadron spectrometer a solid angle of 5.4 msr, a momentum acceptance of $\frac{\delta p}{p} = \pm 4.0\%$ as well as a luminosity of 3.3x10^{35} cm^{-2}s^{-1}. The times for the longitudinal and transverse measurements where determined by optimizing the time sharing for the best precision on the extracted asymmetry A_1. We required an absolute statistical uncertainty $\Delta A_{\parallel}^{^3He} = 0.006$ and $\Delta A_{\perp}^{^3He} = 0.015$ and corrected for the target and beam polarizations.

The absolute uncertainty $\Delta A_1^{^3He}$ is obtained by propagating the uncertainty from $A_{\parallel}^{^3He}$ and $A_{\perp}^{^3He}$ to $A_1^{^3He}$ using equations (16,17). Fig. 7 (a) shows the projected electron and pion cross sections, where the pion cross sections were generated using the O'Connell and Lightbody code EPCV and (b) the projected results for the ^{3}He asymmetry $A_1^{^3He}$ and for the neutron asymmetry A_1^n.

To evaluate the systematic uncertainty of the corrected asymmetry we used $\Delta P_b/P_b = 0.03$ achieved during E94-010 and E95-001 and $\Delta P_t/P_t = 0.05$, which is the projected relative uncertainty of E94-010. The total uncertainty in $A_1^{^3He}$ is dominated by the statistical rather than the systematic uncertainty over the full x range of the measurement.

An elastic scattering asymmetry measurement is planned at small energies (E_i = 1.6 GeV $\theta = 15°$) in order to measure the product of the target density and polarization. This quantity can be evaluated using the measured electric and magnetic form factors of ^{3}He. This measurement would actually determine the polarization of the ^{3}He nuclei along the electron beam path. False asymmetries will be checked to be consistent with zero by comparing data with target spins in opposite directions.

Also contributing to the dilution of the asymmetry is the pair-electron contamination. This correction is x dependent, and is relevant only in the lowest x bins region. This contamination was estimated to be no more than 6% in the worst case. It will be measured by reversing the spectrometer polarity.

Table 1: Summary of the kinematics, times and rates of the proposed measurement. It should be noted that the statistical uncertainties are obtained when using combined data from both spectrometers.

E' (GeV)	x	Q^2 $(\mathrm{GeV})^2$	D	W^2 (GeV)	$A_1^{^3He}$	$\Delta A_1^{^3He}$	$A_2^{^3He}$	$\Delta A_2^{^3He}$	Rate Hz	time$_\parallel$ Hours	time$_\perp$ Hours
1.51	.63	5.3	.85	2.0	0.062	0.0077	0.033	0.0229	0.171	220	35
1.30	.52	4.6	.87	2.3	0.031	0.0073	0.014	0.0235	0.290	130	21
1.10	.42	3.9	.90	2.5	0.013	0.0069	0.005	0.0244	0.402	94	15
0.90	.33	3.2	.92	2.7	-0.004	0.0067	-0.001	0.0257	0.492	77	13

2.4.1 Radiative corrections

The radiative corrections (RC) will be performed in two stages. First the internal corrections will be evaluated following the procedure developed by Bardin and Shumeiko[30] for the unpolarized case and extended to the spin dependent lepto-production cross sections by Akushevish and Shumeiko[31, 32]. Second, using these internally corrected cross sections, the external corrections (for thick targets) are applied by extending the procedure developed for the unpolarized cross sections by Tsai[33, 34] with modifications appropriate for this experiment. Because of the relatively thin target entrance window ($\sim 0.3\%$ radiation length) combined with the exit window thickness of 1 mm ($0.7\mathrm{mm}/\sin 45^\circ \sim 0.8\%$ r. l.) we expect the external corrections to be small. We point out that all corrections will be carried on the measured parallel $A_\parallel$ and perpendicular $A_\perp$ asymmetries. A_1 is extracted only at the end of the procedure using the required kinematical factors.

The internal corrections will be carried using the program **Polrad version 15** in its iterative method version. In this method the best fit to the experimental asymmetry of ^{3}He is used as a first input to the iterative procedure. The corrected asymmetry is then fitted and used as input to the next iteration step. The process is repeated until convergence is reached, which occurs within four to five steps.

The nuclear coherent elastic tail was evaluated using different best fits to the elastic form factors of ^{3}He. The effect on the asymmetry was found to be negligible even at the lowest value of x. This leaves only three physical regions making significant contributions to the total internal radiative correction; The quasielastic region; the resonance region and the deep inelastic region. The quasielastic region begins a few MeV beyond the elastic peak since ^{3}He has no excited states. The beginning of the resonance region is somewhat ill defined due to the merging of the quasielastic and resonance tails. The deep inelastic region is assumed to begin at $W = 2$ GeV.

The RC require the knowledge of the spin independent structure functions (SISF) $W_1^{^3He}(Q^2,\nu)$ and $W_2^{^3He}(Q^2,\nu)$ and spin dependent structure functions (SDSF) $G_1^{^3He}(Q^2,\nu)$ and $G_2^{^3He}(Q^2,\nu)$ over the canonical triangle region[34]. The lowest x bin in this measurement ($x = 0.3$) requires the knowledge of the structure functions over the full kinematical range of Q^2 and x. It extends in the range 10 GeV $\leq Q^2 \leq 2.5$ GeV and $0.3 \leq x \leq 1$. These variables are converted to the proper integration variables for the RC method defining the canonical triangle given by M_x and t where $M_n + m_\pi \leq M_x \leq W$ and $t_{min} \leq t \leq t_{max}$; $t \equiv Q^2$.

The SISF used in the quasielastic region were those of de Forest and Walecka [35]. These structure functions are not the best available but allow an easy parameterization for a reasonably accurate and fast evaluation of the unpolarized radiative tail. In the resonance region we chose the SISF obtained with careful fitting of data from Ref.[36]. For the deep inelastic region, where previous SLAC measurements were performed, the Whitlow global fit [37] was the preferred model for the SISF. Except for the quasielastic region the effect of Fermi motion is only partially included

Table 2: Internal Radiative corrections effects using **Polrad 15**. Iteration 5 is the final Born asymmetry while Raw is the measured asymmetry.

E' (GeV)	x	Q^2 (GeV)^2	D	W^2 (GeV)	$A_{1r}^{^3He}$ (Raw)	$A_{1c}^{^3He}$ (Iter 1.)	$A_{1c}^{^3He}$ (Iter 3.)	$A_{1c}^{^3He}$ (Iter 5.)	$\Delta A_1^{^3He}$ (Iter. 5-Raw)
1.51	.63	5.3	.85	2.0	0.0619	0.0442	0.0454	0.0402	0.0217
1.30	.52	4.6	.87	2.3	0.0313	0.0238	0.0243	0.0248	0.0065
1.10	.42	3.9	.90	2.5	0.0135	0.0064	0.0061	0.0116	0.0019
0.90	.33	3.2	.92	2.7	-0.0042	-0.0137	-0.0149	-0.0072	0.0030

in the evaluation of the deep inelastic structure functions. In other words ^{3}He is considered as made of a deuteron and a proton at rest, so the only spread due to the motion of the nucleons in ^{3}He is represented only by the deuterium width of the quasielastic peak. In the resonance region the SDSF used were obtained from the AO program which is based on an analysis of electromagnetic transition amplitudes in the resonance region[38], while in the deep inelastic region a fit to the extracted $A_1^{^3He}$ from the SLAC experiment[1] E142 was used.

In table 2 we have evaluated the radiative corrections to the asymmetry through five iterations as an estimate of the magnitude of this correction. The correction adds at most $\pm 2\%$ in absolute value to the asymmetry at the highest x bin. The study of systematic effects on the radiative corrections due to model dependence of the SISF and SDSF is still under investigation.

2.4.2 From ^{3}He to a Neutron

The determination of the inelastic spin-dependent structure function of the neutron from a measurement on ^{3}He relies on our understanding of the reaction mechanism of the virtual photon combined with the use of a realistic ^{3}He wave function. Detailed investigations of the ^{3}He inelastic spin response functions versus that of a free neutron have been carried out by three expert groups in few-body problems[39, 40, 41]. They examined the effect of the Fermi motion of nucleons and their binding in ^{3}He along with the study of the electromagnetic interaction treatment using the most realistic ^{3}He wave function.

In the deep inelastic region an effective neutron spin structure response can be extracted to first order from that of ^{3}He using a procedure in which S, S' and D states of the ^{3}He wave function are included, but no Fermi motion or binding effects are introduced:

$$\widetilde{g}_1^n = 1/\rho_n (g_1^{^3He} - 2\rho_p g_1^p) \tag{35}$$

$$\widetilde{A}_1^n = \frac{W_1^{^3He}}{W_1^n}\frac{1}{\rho_n}(A_1^{^3He} - 2\frac{W_1^p}{W_1^{^3He}}\rho_p A_1^p) \tag{36}$$

where $\widetilde{g}_1^n$, g_1^p and $g_1^{^3He}$ are the spin structure functions of an effective free neutron, a free proton and ^{3}He, respectively. Similarly $\widetilde{A}_1^n$, A_1^p and $A_1^{^3He}$ are the photon-target asymmetries for an effective free neutron, a free proton and ^{3}He, respectively. $\rho_n = (87 \pm 2)\%$ and $\rho_p = (-2.7 \pm 0.3)\%$ are the polarization values of the neutron and proton in ^{3}He due to the S, S' and D states of the wave function [40]. The Convolution approach calculations using the "exact" ^{3}He wave function

Table 3: Uncertainties in the extraction of the neutron asymmetry from the measurement of ^{3}He.

E' (GeV)	x	Q^2 (GeV)^2	W (GeV)	D	$A_1^{^3He}$	$\Delta A_1^{^3He}$ (stat.)	$\Delta A_1^{^3He}$ (syst.)	$\Delta A_1^{^3He}$ (total)	A_1^n	ΔA_1^n (total)
1.51	.63	5.31	2.00	.85	0.062	0.0077	0.0033	0.0084	0.375	0.064
1.30	.52	4.57	2.26	.87	0.031	0.0073	0.0017	0.0075	0.249	0.056
1.10	.42	3.87	2.49	.90	0.014	0.0069	0.0007	0.0070	0.129	0.049
.90	.33	3.16	2.70	.92	-0.004	0.0067	0.0002	0.0067	0.026	0.043

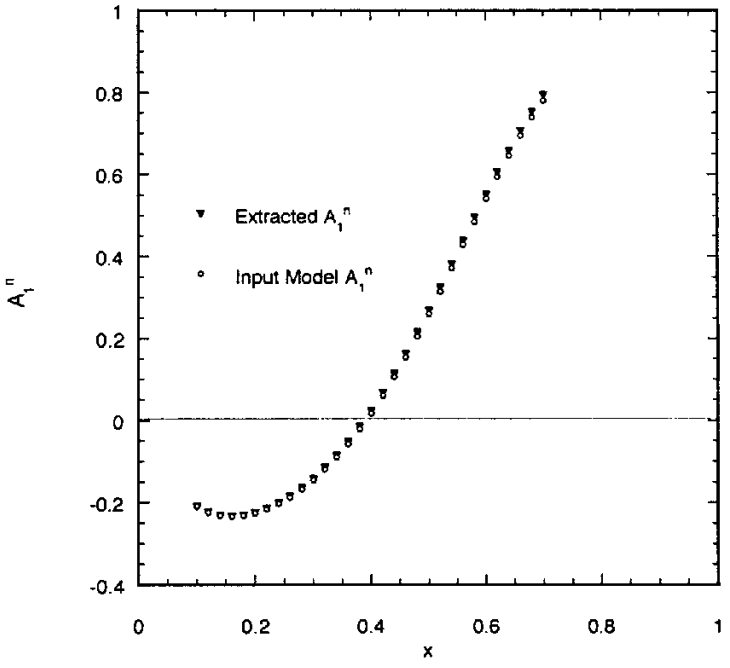

Figure 8: Neutron asymmetry input used in the complete convolution method ref [40] compared to the neutron asymmetry extracted using the method described in the same reference.

Table 4: Summary of parameters for the proposed experiment

E' (GeV)	x	Q^2 $(\mathrm{GeV})^2$	W (GeV)	D	$A_1^{^3He}$	Rate Hz	time$_\parallel$ Hours	time$_\perp$ Hours	A_1^n	ΔA_1^n (total)
1.51	.63	5.31	2.00	.85	0.062	0.171	220	35	0.27	0.064
1.30	.52	4.57	2.26	.87	0.031	0.290	130	21	0.20	0.056
1.10	.42	3.87	2.49	.90	0.014	0.402	94	15	0.12	0.049
.90	.33	3.16	2.70	.92	-0.004	0.492	77	13	0.005	0.043

including the full treatment of Fermi motion and binding effects show negligible differences with the above approximation8.

In our analysis we shall use the full convolution method to extract the neutron asymmetry. A precise proton measurement is important to minimize the error on the correction. From the presently available proton asymmetry data (SLAC E-80, E-130, E143, CERN, EMC, HERMES, SMC) and that of the neutron (E-142, SMC, E154, HERMES) we can state that the uncertainty due to nuclear effects is not the dominant contribution to the error. At worst, it adds an absolute uncertainty of $\Delta A_1 \sim 2\%$ to the measured asymmetries at the highest x bin.

In summary, we extract the neutron asymmetry from the measured ^{3}He asymmetry, following the method described in Ref.[40], where Fermi motion, binding effects and S, S' and D states of the wave function are included.

In Table 3, we used the statistical and systematic uncertainties of the projected ^{3}He measurement, to produce the neutron asymmetry and its total uncertainty. We includes to first order the corrections due to the polarization of the two protons in ^{3}He ($\sim -2.7\%$ per proton) and for the polarization of the neutron in ^{3}He ($\sim$87%) following equation 36.

3 Summary and Beam Request

In summary, we propose to carry out a precision determination of the neutron asymmetry A_1^n in the large x region ($0.33 \leq x \leq 0.63$) (see Fig 9) from a measurement using a high pressure polarized ^{3}He target (P_t= 40%) and the presently highest available energy (6 GeV) polarized beam(P_b=80%). This measurement requires 521 hours of beam on target for the measurement of the longitudinal asymmetry and 84 hours for the measurement of the transverse asymmetry, along with 120 hours for spectrometer momentum changes, positron measurements in the lowest two x bins, elastic scattering calibration and beam and target polarization measurements. We therefore request a total of 725 hours (30 days) of beam time.

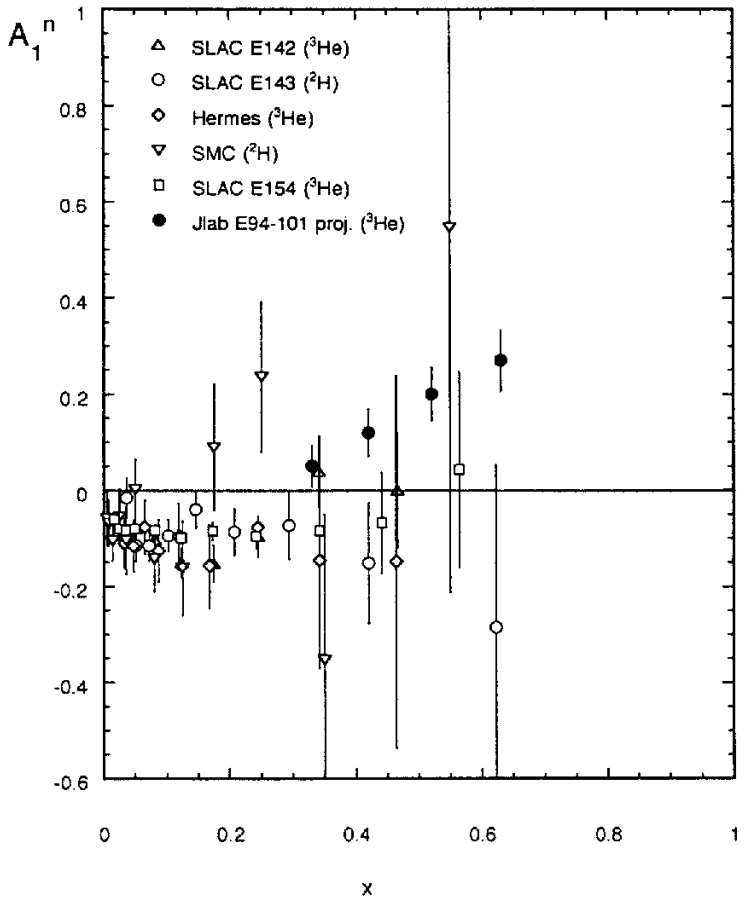

Figure 9: The World data of A_1^n neutron versus x from Ref.[1, 2, 3, 4, 5] and the projected data from this proposal. The projected data on the figure assume a central value of Isgur model [14].

[1] The SLAC E142 collaboration, P. Anthony et al., Phys. Rev. Lett. **71** (1993) 959; Phys. Rev. D**54** (1996) 6620.

[2] B. Adeva et al., Phys. Lett. B**362** (1993) 352.

[3] The E143 collaboration, K. Abe *et al.*, Phys. Rev. Lett. **74** 25 (1995) 346; Phys. Rev. Lett. **75** (1995) 25.

[4] The HERMES collaboration, K. Ackerstaff *et al.*, Phys. Lett. **B404** (1997) 383.

[5] The E154 collaboration, K. Abe *et al.*, Phys. Rev. Lett. **79** (1997) 26.

[6] R. Feynman, *Photon Hadron Interactions*, (Benjamin New York, 1972), p. 150.

[7] F. Close, Phys. Lett. **B43**, 422 (1973); Nucl. Phys. **B80**,269 (1974) and *An introduction to Quarks and Partons* (Academic Press, N. Y., 1979), p. 197.

[8] M.J. Alguard et al., Phys. Rev. Lett. **37** (1976) 1258; **37** (1976) 1261.

[9] G, Baum et al., Phys. Rev. Lett. **51** (1983) 1135.

[10] J. Ashman et al., Phys. Lett. B**206** (1993) 352; Nucl. Phys. B**328** (1989) 1.

[11] The HERMES collaboration, A. Airapetian *et al.*, Phys. Lett. **B442** (1998) 484.

[12] The E155 collaboration, P.L. Anthony *et al.*, hep-exp/9904002, submitted to Phys. Rev. Lett.

[13] R. Carlitz, Phys. Lett. **B 58** (1975)345

[14] N. Isgur, Phys. Rev. **D59** (1999) 034013.

[15] G. R. Farrar and D. R. Jackson, *Phys. Rev. Lett.* **35** (1975) 1416.

[16] G.R. Farrar *Phys. Letters* **70B** (1977) 346.

[17] S. Brodsky, M. Burkhardt and I Schmidt, Nucl. Phys. **B441** (1995) 197.

[18] N. Kochelev, Talk presented at the "Workshop with Polarized Protons at HERA" August 1997 DESY-Zeuthen preprint hep-ph/10540v2

[19] N. Kochelev, private communication

[20] C.E. Carlson and W.-K. Tung, Phys. Rev. D**5**(1972)721.

[21] A.J.G. Hey and J.E. Mandula, Phys. Rev. D**5**(1972)2610.

[22] M.A. Bouchiat, T.R. Carver and C.M. Varnum, Phys. Rev. Lett. **5** (1960)373.

[23] N.D. Bhaskar, W. Happer, and T. McClelland, Phys. Rev. Lett. **49** (1982)25.

[24] W. Happer, E. Miron, S. Schaefer, D. Schreiber, W.A. van Wijngaarden, and X. Zeng, Phys. Rev. A **29** (1984)3092.

[25] T.E. Chupp, M.E. Wagshul, K.P. Coulter, A.B. McDonald, and W. Happer, Phys. Rev. C **36** (1987)2244.

[26] K.P. Coulter, A.B. McDonald, W. Happer, T. E. Chupp, and M.E. Wagshul, Nuc. Inst. Meth. in Phys. Res. **A 270** (1988)90.

[27] N.R. Newbury, A.S. Barton, P. Bogorad, G. D. Cates, M. Gatzke, H. Mabuchi, and B. Saam, Phys. Rev. A **48** (1993)558.

[28] K.P. Coulter, A.B. McDonald, G.D. Cates, W. Happer, T.E. Chupp, Nuc. Inst. Meth. in Phys. Res. A**276** (1989)29 .

[29] A. Abragam, Principles of Nuclear Magnetism (Oxford University Press, New York, 1961).

[30] L. Whitlow, SLAC-report-357(1990).

[31] D. Yu. Bardin and N. M. Shumeiko, Nucl. Phys. **B127** (1977)1251.

[32] T.V. Kuchto and N. M. Shumeiko, Nucl. Phys. **B219** (1983)412.

[33] I. V. Akushevich and N. M. Shumeiko, J. Phys. **G**: Nucl. Part. Phys. **20** (1994)513.

[34] L. W. Mo and Y. S. Tsai, Rev. Mod. Phys. **41** (1969)205.

[35] Y. S. Tsai, SLAC-PUB-848 (1971).

[36] T. De Forest and D.J. Walecka Adv. in Phys. 15(1966)57.

[37] F. W. Brasse, W. Flauger, J. Gauler, S. P. Goel, R. Haiden, M. Merkwitz and H. Wriedt, Nucl. Phys. **B110** (1976)413.

[38] V. Burkert and Z. Li Phys. Rev. D**47** (1993) 46.

[39] B. Blankleider and R.M. Woloshyn, Phys. Rev. C **29** (1984)538.

[40] C. Ciofi degli Atti, S. Scopetta, E. Pace, G. Salme, Phys. Rev. C **49** (1993) R968 .

[41] R.-W. Shulze and P.U. Sauer, Phys. Rev. C**48** (1993)38.